

(even the parent hydrocarbon has  $\Delta G^\ddagger = 12$  kcal/mol at 202 K). Thus, the  $(\text{CH}_2)_8$  loop dramatically accelerates bond shifting. The barrier to ring inversion is also somewhat lower than normal, despite the need to force a vinyl proton through the methylene bridge. This reversal of the normal dynamic properties of [8]-annulenes may open the way for analysis of how bond shifting actually occurs.

**Acknowledgment.** The financial support of the National Science Foundation and the assistance of Dr. Charles Cottrell (Campus Chemical Instrumentation Center) in recording the high field spectra are gratefully acknowledged.

## Correlations between Wettability and Structure in Monolayers of Alkanethiols Adsorbed on Gold<sup>1</sup>

Colin D. Bain<sup>2</sup> and George M. Whitesides\*

Department of Chemistry, Harvard University  
Cambridge, Massachusetts 02138

Received February 29, 1988

Long-chain thiols ( $\text{HS}(\text{CH}_2)_n\text{X}$ ) adsorb from solution onto gold surfaces and form well-packed, ordered, oriented monolayers.<sup>3,4</sup> The sulfur coordinates strongly to the gold, the polymethylene chains are all-trans and tilted  $\sim 20$ – $30^\circ$  from the normal to the surface,<sup>4,5</sup> and the tail group, X, is the predominant group exposed at the monolayer/liquid or monolayer/air interface.<sup>6</sup> Co-adsorption of two or more thiols differing in tail group or chain length provides a flexible system for varying the chemistry and structure of the surface in a controlled and predetermined way.<sup>7</sup> In this paper we use monolayers comprising a mixture of  $\text{HS}(\text{CH}_2)_{11}\text{OH}$  (represented as  $\text{HSC}_{10}\text{CH}_2\text{OH}$  to emphasize the two important variables: chain length and tail group) and  $\text{HS}(\text{CH}_2)_{21}\text{CH}_3$  ( $\text{HSC}_{21}\text{CH}_3$ ) on gold to demonstrate a relationship between the microscopic structure of the surface and the wettability of the monolayer (Figure 1). This work is part of a program of physical–organic chemistry designed to relate atomic-level structure of a surface to macroscopic physical properties such as wetting and adhesion.<sup>8</sup>

Monolayers were formed by immersing gold-mirror substrates (prepared by evaporation of gold onto chromium-primed, polished silicon wafers) in solutions of the thiols in degassed ethanol for 12 h<sup>9</sup> at room temperature.<sup>6</sup> The composition of the monolayer was controlled by varying the ratio  $R = [\text{HSC}_{10}\text{CH}_2\text{OH}] / [\text{HSC}_{21}\text{CH}_3]$  in solution, with the total concentration of thiols held constant at 1 mM. We used two independent techniques, optical ellipsometry and X-ray photoelectron spectroscopy (XPS), to measure the composition of the monolayer. Since the two thiols differ in chain length, the relative thickness obtained from el-

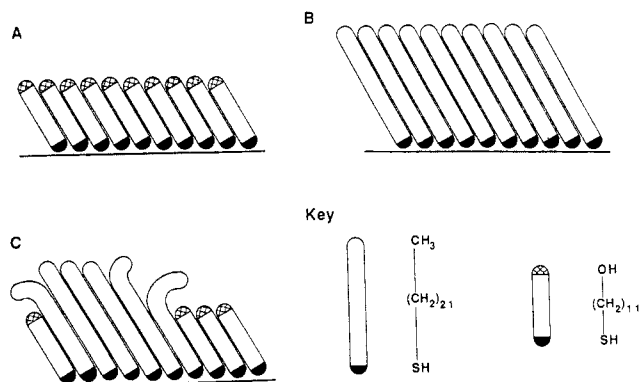


**Figure 1.** Schematic illustrations of monolayer structures: pure  $\text{HS}(\text{CH}_2)_{11}\text{OH}$  (A); pure  $\text{HS}(\text{CH}_2)_{21}\text{CH}_3$  (B); monolayer containing a mixture of the two thiols (C).

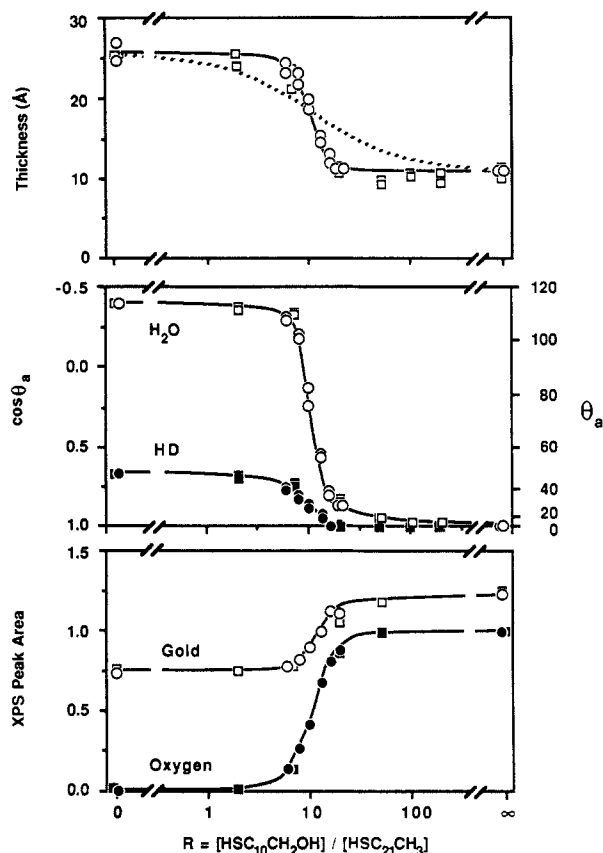


**Figure 2.** Monolayers formed by the adsorption of mixtures of  $\text{HS}(\text{CH}_2)_{11}\text{OH}$  and  $\text{HS}(\text{CH}_2)_{21}\text{CH}_3$  onto gold from solution. The abscissa represents the ratio;  $R = [\text{HS}(\text{CH}_2)_{11}\text{OH}] / [\text{HS}(\text{CH}_2)_{21}\text{CH}_3]$  in solution. Squares and circles represent data from two separate experiments. Upper figure: ellipsometric thickness. The solid curve is a fit to the data. The dotted curve represents the theoretical thicknesses for  $K_{\text{eq}} = 11$  (see text for definition). Middle figure: advancing contact angles of water (open symbols) and hexadecane (HD) (solid symbols) obtained by the sessile drop technique. Lower figure: areas of the Au ( $4f_{7/2}$ ) (open symbols) and O ( $1s$ ) peaks (solid symbols) obtained by XPS. The vertical scale is arbitrary. Data were collected on a SSX-100 X-ray photoelectron spectrometer (Surface Science Instruments) with a monochromatized Al-K $\alpha$  source, 100 eV pass energy, and 1-mm X-ray spot. The peaks were fitted with a symmetrical 90% Gaussian/10% Lorentzian profile.

lipsometry and from the peak area of gold<sup>10</sup> in XPS reflects this composition. Similarly, the difference in tail groups allows us to calculate the surface concentration of  $\text{HSC}_{10}\text{CH}_2\text{OH}$  from the peak area of oxygen. The advancing contact angles ( $\theta_a$ ) of water

(1) Supported in part by the Office of Naval Research and the Defense Advanced Research Projects Agency. XPS spectra were obtained with facilities obtained through the DARPA/URI and maintained in the Harvard University Materials Research Laboratory.

(2) IBM Pre-Doctoral Fellow in Physical Chemistry 1985–1986.

(3) Nuzzo, R. G.; Allara, D. L. *J. Am. Chem. Soc.* **1983**, *105*, 4481–4483. Strong, L.; Whitesides, G. M. *Langmuir*, in press.

(4) Porter, M. D.; Bright, T. B.; Allara, D. L.; Chidsey, C. E. D. *J. Am. Chem. Soc.* **1987**, *109*, 3559–3568.

(5) Nuzzo, R. G.; Dubois, L. H.; Allara, D. L., unpublished results.

(6) Bain, C. D.; Troughton, E. B.; Tao, Y.-T.; Evall, J.; Whitesides, G. M.; Nuzzo, R. G. *J. Am. Chem. Soc.*, submitted for publication.

(7) Bain, C. D.; Whitesides, G. M. *Science (Washington, D.C.)* **1988**, *240*, 62–63.

(8) Troughton, E. B.; Bain, C. D.; Whitesides, G. M.; Nuzzo, R. G.; Allara, D. L.; Porter, M. D. *Langmuir* **1988**, *4*, 365–385. Holmes-Farley, S. R.; Reamey, R. H.; McCarthy, T. J.; Deutch, J.; Whitesides, G. M. *Langmuir* **1985**, *1*, 725–40. Holmes-Farley, S. R.; Whitesides, G. M. *Langmuir* **1986**, *2*, 266–281. Holmes-Farley, S. R.; Whitesides, G. M. *Langmuir* **1987**, *3*, 62–75. Holmes-Farley, S. R.; Reamey, R. H.; Nuzzo, R. G.; McCarthy, T. J.; Whitesides, G. M. *Langmuir* **1987**, *3*, 799–815. Holmes-Farley, S. R.; Bain, C. D.; Whitesides, G. M. *Langmuir*, in press.

(9) For pure thiols, initial monolayer formation is very rapid ( $\sim$  few seconds) with limiting properties reached after a few hours.

(10) The intensity of the photoelectron peak decreases exponentially with the thickness of the monolayer due to inelastic scattering of the photoelectrons (Briggs, D.; Seah, M. P. *Practical Surface Analysis*; Wiley: Chichester, 1983).

and hexadecane (HD) provide useful measures of wettability. Since the pure methyl-terminated monolayer is hydrophobic ( $\theta_a(\text{H}_2\text{O}) = 114^\circ$ ,  $\theta_a(\text{HD}) = 48^\circ$ ), and the alcohol-terminated monolayer is hydrophilic ( $\theta_a(\text{H}_2\text{O}) = \theta_a(\text{HD}) \approx 0^\circ$ ), contact angles are very sensitive to the composition of the monolayer and the structure of the surface.

Figure 2 plots the ellipsometric thickness, contact angles of water and hexadecane, and XPS peak areas of gold and oxygen against  $R$ .<sup>11</sup> Here we note two salient features of these graphs: a detailed discussion will be deferred to a subsequent paper. First, ellipsometry and XPS peak areas indicate a dramatic change in the composition of the monolayer over a narrow range of solution composition,  $R = 7$ –20. This change in the composition of the monolayer is closely correlated with a sharp increase in the hydrophilicity and oleophilicity of the surface as measured by the advancing contact angles of water and hexadecane, respectively.<sup>12</sup> Thus the structure of the surface on a microscopic scale is clearly and directly linked to the wettability of the monolayer, an important macroscopic quantity. Second, the inflection in the curves occurs, not at  $R = 1$ , but at  $R \approx 11$ .<sup>13,14</sup> This difference between solution and surface compositions is a general feature of competitive adsorption experiments.<sup>15</sup> In this experiment, van der Waals forces between close-packed hydrocarbon chains favor adsorption of the longer chain thiol.

We attempted to model the composition of the monolayer by a simple equilibrium expression (eq 1) between the solution and the surface (dotted curve in Figure 2, upper graph) where the

$$\text{HSC}_{10}\text{CH}_2\text{OH}_{\text{surface}} + \text{HSC}_{21}\text{CH}_3_{\text{solution}} \rightleftharpoons \text{HSC}_{10}\text{CH}_2\text{OH}_{\text{solution}} + \text{HSC}_{21}\text{CH}_3_{\text{surface}} \quad (1)$$

equilibrium constant  $K_{\text{eq}} = 11$ , independent of solution concentration. Clearly the observed data do not follow this simple expression: the two components of the monolayer do not act independently and may act cooperatively to minimize the free energy. Monolayers composed predominantly of the long-chain methyl-terminated thiol  $\text{HSC}_{21}\text{CH}_3$  (maximizing the chain-packing interactions) or the short-chain hydroxy-terminated thiol  $\text{HSC}_{10}\text{CH}_2\text{OH}$  (maximizing H-bonding both with the solvent and within the monolayer) are preferred over monolayers containing a mixture of the thiols.<sup>16</sup> The data do not, however, take the form of step functions in  $R$ , which would be expected thermodynamically if the formation of macroscopic islands were favored.<sup>17</sup> Over a narrow range of  $R$  it is possible to form intermediate monolayers containing both thiols; the exact structure of these monolayers is not clear, but the data are consistent with a model in which the two components segregate into small clusters on the surface. These monolayers provide a model system for studying the wettability of complex structures and for examining how polar groups interact to minimize their energy in a nonpolar environment.<sup>18</sup>

Mixed monolayers of thiols on gold allow us to engineer ordered, two-dimensional systems with Å-level control over thickness and

structure and with chemical control over wettability. Synthetic variation of the tail groups and chain lengths provides great flexibility in the design of the interfacial structures and gives these systems wide applicability in the physical, biological, and medical sciences.

**Acknowledgment.** We are grateful to R. Nuzzo and M. Wrighton for helpful discussions.

**Registry No.**  $\text{HS}(\text{CH}_2)_{11}\text{OH}$ , 73768-94-2;  $\text{HS}(\text{CH}_2)_{21}\text{CH}_3$ , 7773-83-3; Au, 7440-57-5.

### Novel Triple Cubane-Type Organometallic Oxide Clusters: $[\text{MCp}^*\text{MoO}_4]_4 \cdot n\text{H}_2\text{O}$ ( $\text{M} = \text{Rh}$ and $\text{Ir}$ ; $\text{Cp}^* = \text{C}_5\text{Me}_5$ ; $n = 2$ for $\text{Rh}$ and 0 for $\text{Ir}$ )

Yoshihito Hayashi, Koshiro Toriumi,\* and Kiyoshi Isobe\*

*Institute for Molecular Science  
Myodaiji, Okazaki 444, Japan*

*Received December 8, 1987*

In recent years there has been a growing interest in the metal oxide clusters containing organometallic groups and polyoxoanions, a field which has been developed by W. G. Klemperer, W. Knoth, and R. G. Finke.<sup>1</sup> These novel clusters provide models for metal oxide surfaces which are catalysts for a variety of hydrocarbon transformations, and they represent a meeting point for the chemistry of low-valent and high-valent transition metals. This communication reports structures and properties of newly prepared organometallic oxide clusters possessing a novel triple cubane framework.

Aqueous solution (5 cm<sup>3</sup>, pH 7.3) of  $\text{Na}_2\text{MoO}_4 \cdot 2\text{H}_2\text{O}$  (2.0 g,  $8.3 \times 10^{-3}$  mol) was added dropwise to a suspension of (partially dissolved)  $[\text{RhCp}^*\text{Cl}_2]_2$  (0.5 g,  $8.0 \times 10^{-4}$  mol) in water (3 cm<sup>3</sup>, pH ca. 3.8), and the mixture was stirred at 25 °C for 3 h to deposit a yellow-orange solid. In the case of  $[\text{IrCp}^*\text{Cl}_2]_2$ , a yellow solid was obtained after refluxing at 100 °C for 1 h. These products were recrystallized from  $\text{CH}_2\text{Cl}_2$ – $\text{C}_6\text{H}_5\text{Me}$  (1:1 by volume) with 93% and 68% yields for  $\text{Rh}$  (red crystals) and  $\text{Ir}$  (yellow crystals) complexes, respectively. Both new complexes gave satisfactory analyses and molecular weights for the molecular formula  $[\text{M}(\text{C}_5\text{Me}_5)\text{MoO}_4]_4 \cdot n\text{H}_2\text{O}$  ( $n = 2$  for  $\text{M} = \text{Rh}$  (1) and 0 for  $\text{Ir}$  (2)); and the water of crystallization is easily lost under vacuum at room temperature.<sup>3</sup> These complexes are soluble in most organic solvents except hydrocarbons. The rhodium complex is also slightly soluble in water and shows a molar conductivity of 75.9 S cm<sup>2</sup> mol<sup>−1</sup> (concentration of complex:  $4.35 \times 10^{-4}$  mol dm<sup>−3</sup>) at 25 °C. X-ray photoelectron spectra of 1 and 2 show the oxidation states of the Mo, Rh, and Ir atoms to be +6, +3, and +3, respectively (binding energies, Mo 3d<sub>5/2</sub>: 231.4 (for 1), 231.3 eV (for 2); Rh 3d<sub>5/2</sub>: 308.8 eV; Ir 4f<sub>7/2</sub>: 61.7 eV).<sup>4</sup>

(11) We prefer  $\log R$  to the mole fraction,  $\chi$ , as the abscissa because  $kT \log R$  is related to the Gibbs free energy, and hence this choice of axis highlights thermodynamic contributions to the adsorption process.

(12) Hexadecane and water interact predominantly by dispersion and polar forces, respectively. The detailed inferences from the contact angle data and comparisons with other monolayer systems will be discussed in a subsequent paper.

(13) The ellipsometric thickness yields a value of  $R(\chi_{1/2}) = 11$  where  $\chi_{1/2} = 1:1$  ratio of the two thiols in the monolayer. XPS peak areas yield  $R(\chi_{1/2}) = 10$ –12 depending on the model used to analyze the data.

(14) The monolayer system had not quite reached equilibrium when these measurements were made. Over a period of 2 weeks  $R(\chi_{1/2})$  slowly increased to  $R \approx 14$ .

(15) Bain, C. D.; Whitesides, G. M., unpublished results.

(16) Despite being enthalpically disfavored, some  $\text{HSC}_{21}\text{CH}_3$  is incorporated into the  $\text{HSC}_{10}\text{CH}_2\text{OH}$  monolayer even at large  $R$  (and vice versa) due to the favorable entropy of mixing.

(17) We believe that absorption of thiols onto gold is controlled to a large extent by thermodynamics, although kinetics also play a role, as evinced by the slow change in the monolayer composition with time after the initial, rapid absorption.

(18) Israelachvili, J. N. *Intermolecular and Surface Forces*; Academic: New York, 1985.

(1) (a) Day, V. W.; Klemperer, W. G. *Science (Washington, D.C.)* **1985**, *228*, 533–541. (b) Domaille, P. J.; Knoth, W. H. *Inorg. Chem.* **1983**, *22*, 818–822. (c) Finke, R. G.; Rapko, B.; Domaille, P. J. *Organometallics* **1986**, *5*, 175–178. (d) Muetterties, E. L. *Chem. Eng. News: Special Report* **1982**, Aug. 30, pp 28–41. (e) Pope, M. T. "Heteropoly and Isopoly Oxometalates" In *Inorganic Chemistry Concepts No. 8*; Springer-Verlag: Berlin, Heidelberg, New York, Tokyo, 1983; pp 118–127.

(2) Kang, J. W.; Moseley, K.; Maitlis, P. M. *J. Am. Chem. Soc.* **1969**, *91*, 5970–5977.

(3) 1: Anal. Calcd for  $\text{C}_{40}\text{H}_{64}\text{Mo}_4\text{O}_{18}\text{Rh}_4$  (dihydrate): C, 29.51; H, 3.96. Found: C, 30.17; H, 3.80; mol wt calcd for anhydrous 1 1592, found 1480. 2: Anal. Calcd for  $\text{C}_{40}\text{H}_{60}\text{Ir}_4\text{Mo}_4\text{O}_{16}$ : C, 24.64; H, 3.10. Found: C, 24.56; H, 3.11; mol wt calcd 1949, found 1860. The molecular weights were determined by vapor pressure osmometry in dichloromethane at 27 °C.

(4) The corresponding values of binding energy in the starting materials,  $\text{Na}_2\text{Mo}^{\text{VI}}\text{O}_4 \cdot 2\text{H}_2\text{O}$  (Mo 3d<sub>5/2</sub>, 231.5 eV),  $[\text{Rh}^{\text{III}}\text{Cp}^*\text{Cl}_2]_2$  (Rh 3d<sub>5/2</sub>, 308.3 eV), and  $[\text{Ir}^{\text{III}}\text{Cp}^*\text{Cl}_2]_2$  (Ir 4f<sub>7/2</sub>, 61.3 eV) are very close to those in 1 and 2. Observed values were corrected by assuming  $\text{C}_{1s}$  binding energy in  $\text{Cp}^*$  rings of 1 and 2 as 284.6 eV.